# Experimental study on pressure, stress state, and temperature-dependent dynamic behavior of shear thickening fluid subjected to laser induced shock

Xianqian Wu, Qiuyun Yin, and Chenguang Huang

Citation: Journal of Applied Physics **118**, 173102 (2015); doi: 10.1063/1.4934857
View online: http://dx.doi.org/10.1063/1.4934857
View Table of Contents: http://scitation.aip.org/content/aip/journal/jap/118/17?ver=pdfcov
Published by the AIP Publishing

# Experimental study on pressure, stress state, and temperature-dependent dynamic behavior of shear thickening fluid subjected to laser induced shock

Xianqian Wu,[a] Qiuyun Yin, and Chenguang Huang
*Key Laboratory of Mechanics in Fluid Solid Coupling Systems, Institute of Mechanics, Chinese Academy of Sciences, Beijing 100190, People's Republic of China*

(Received 24 July 2015; accepted 18 October 2015; published online 4 November 2015)

The dynamic response of the 57 vol./vol. % dense spherical silica particle-polyethylene glycol suspension at high pressure was investigated through short pulsed laser induced shock experiments by measuring the back free surface velocities of aluminum-shear thickening fluid (STF)-aluminum assembled targets. The results showed that the attenuation behavior of shock wave in the STF was dependent on shock pressure, stress state, and test temperature. The measured back free particle velocities of the targets and shock wave velocities in the STF decreased with the decrease in shock pressure while shocked at the same stress state and the same test temperature. In addition, two types of dragging mechanisms in the STF were observed while shocked at different stress states. For a uniaxial strain state, the impact induced jamming behavior in the STF is the dragging mechanism for the attenuation of shock wave, and a critical shock pressure was required for the impact induced thickening behavior. However, while the shock wave transformed from a uniaxial strain state to a dilatation state after transmitted to a certain distance, beside the dragging effect of impact induced jamming behavior, a strong dragging effect, induced by shear induced thickening behavior, was also observed. © *2015 AIP Publishing LLC*. [http://dx.doi.org/10.1063/1.4934857]

## I. INTRODUCTION

Impact resistance and explosive protection of materials have attracted great attention for many years. Many kinds of materials, such as ceramics,[1,2] porous foam metals,[3,4] and granular materials,[5–7] are found to show an excellent high impact resistance and energy absorption behavior at high pressures and high strain rates. However, the energy absorption behavior of these kinds of materials is irreversible, i.e., the impact resistances of these materials are partially or almost completely lost after a single severe impact. For instance, during an impact with high impulse energy, most of the porous foam metals will experience a large plastic deformation and will be crashed eventually. Although the granular materials like sand absorb most of the impact energy through the friction of boundary layers and elastic deformation of particles, some of the particulates will crack into pieces at a high impact pressure. The irreversible energy absorption behavior restricts the applications of these materials in some engineering structures subjected to multiple impacts, and therefore, some smart materials with reversible energy absorption behavior are required in this situation.

Shear thickening fluid (STF) is one kind of smart materials that shows a reversible energy absorption behavior.[8–10] In addition, STF shows an excellent energy absorption capacity through the viscous dissipation during the transition from a fluid-like state to a solid-like state, i.e., shear thickening behavior by shear deformation.[9,11–13] It has been regarded as a kind of advanced materials for designing composite materials and structures with a high impact resistance. The shear thickening is a non-Newton behavior in which the viscosity of fluid increases with shear stress or shear rate. In addition, a minimum shear strain is also found to be required for the shear thickening behavior. The shear thickening behavior is observed to be the result of rearrangement of particles from an ordered state to a disordered state, e.g., formation of jamming particle clusters during shear loading.[9,13] When shear loading is removed, the viscosity of fluid recovers rapidly to its initial state.[13] Due to the excellent energy absorption behavior, STF has found applications in a variety of fields such as armors,[14–17] dampers,[18] to name a few. There is a considerable body of knowledge in the literature that addresses the impact resistance of composite impregnated with STFs during knife spike and ballistic penetration, and high spike/impact resistances of these composites are observed.

Since the impact resistance of STFs is dynamic by nature, it is important to better understand the dynamic response of the suspensions itself under impulse loading. Some of researches have been performed to address the dynamic behavior of STF at various pressures and loading rates. Lim *et al.*[19] investigated the dynamic response of viscosity fluids through a modified split Hopkinson pressure bar (SHPB). The viscosities of shear thickening fluids with various volume fractions were analyzed from stress versus strain curves based on a modified squeezing flow model, and a rate dependent constitutive mode was obtained for STF. Waitukaitis and Jaeger[9] studied the dynamic solidification behavior of STF by directly dropping a metal rod into the STF specimens. The results showed that during the stresses originated from an impact-generated solidification front that transformed an initially compressible particle matrix into a rapidly growing jammed region, extraordinary amount of momentum was absorbed. Recently, Jiang *et al.*[8] studied the

[a]Author to whom correspondence should be addressed. Electronic mail: wuxianqian@imech.ac.cn. Tel.: 86-10-8254 4256.

 

energy absorption behavior of STF using a modified SHPB setup. The relationship between the input energy and the output energy was obtained according to the incident wave and transmitted wave, respectively, and the displacement of the STF specimens during the impact was also obtained. However, the aforementioned studies on the impact resistance of STF have been limited to relatively low pressures. Our recent study[20] on the dynamic response of STF subjected to laser induced shock with a peak pressure up to several GPa showed that the shock and the particle velocities, the shock pressure, and the shock energy decreased rapidly while propagating through a thin layer of STF. Saturation behaviors of the shock attenuation and the energy absorption of the STF were observed. Further studies are needed to investigate the dynamic response of STF at various shock pressures, stress sates, and temperatures to better understand the impact resistance of STF under various impulse loadings, such as ballistic penetration and explosive loadings, and at various ambient temperatures.

With this as a motivation, an experimental study was undertaken at the Institute of Mechanics, Chinese Academy of Sciences, to better understand the dynamic mechanical behavior of shear thickening fluid at various shock pressures and temperatures. In this study, the thin disk shaped STF specimens sandwiched between two aluminum plates were shocked implemented by the interaction between high power density laser and metals. Various shock pressures were achieved by changing the incident laser energy and the laser diameter. The dynamic response of STF was diagnosed from the back free surface velocities. The shock pressure, stress state, and temperature dependent dynamic behavior of STF were systematically investigated.

The paper is organized as follows. In Section II, the experimental procedure used for preparing the STF specimens as well as the laser induced shock loading method at various temperatures is described. In Section III, the experimental details and corresponding experimental results on STF are provided. In Section IV, the dynamic response of STF at various shock pressures and temperatures is compared, and the discussion relevant to the experimental results is provided.

## II. EXPERIMENTAL METHODS

The dynamic behavior of STF at high pressures was studied by laser induced shock experiments equipped with an *in-situ* shock diagnostic system for measuring back free surface velocities as depicted in Fig. 1. In a typical laser induced shock process,[21–23] followed by a beam of high power density laser irradiating an absorption layer glued on a metallic target surface through a sheet of transparent overlay, a thin surface layer of the metallic target is heated and transformed rapidly into the plasma state with high electron and ion densities that are constrained between the transparent overlay and the remaining part of the target. Generally, the plasma peak pressure reaches up to several GPa in tens of nanoseconds, and it drops quickly due to its rapid adiabatic expansion after the laser switches off.[21,23–26] Various peak pressures can be achieved by adjusting the incident laser power density. While the laser induced shock pressure

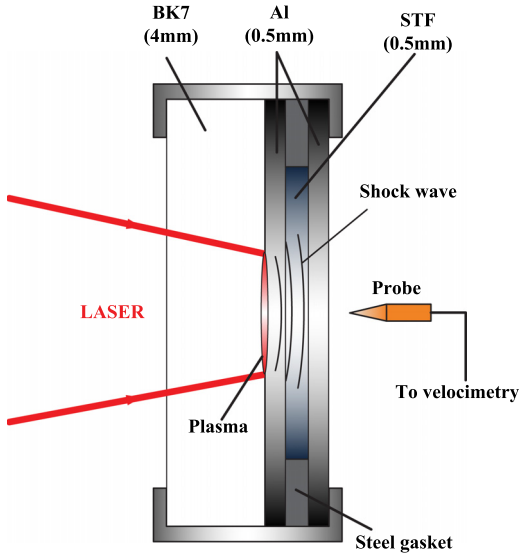


FIG. 1. Schematic of laser induced shock experiments. The shock wave with an amplitude of several GPa and a tens of nanoseconds duration is generated through the laser-matter interaction. A velocimetry is used to capture the back free surface of the target.

propagates through the target, the back free surface velocity of the target is measured by a velocimetry, from which the dynamic response of STF at various pressures, temperatures, and stress state can be analyzed.

### A. STF specimens

The STF studied in this paper is based on silica sphere particles and polyethylene glycol with a particle volume fraction of 57%. As shown in Fig. 2, the silica sphere particles are nearly monodisperse with an average diameter of 300 nm with less than 10% polydispersity. These silica sphere particles were oven dried and suspended uniformly in polyethylene glycol through a combination of hand mixing and ultrasonic vibrator. The densities of the silica particles and

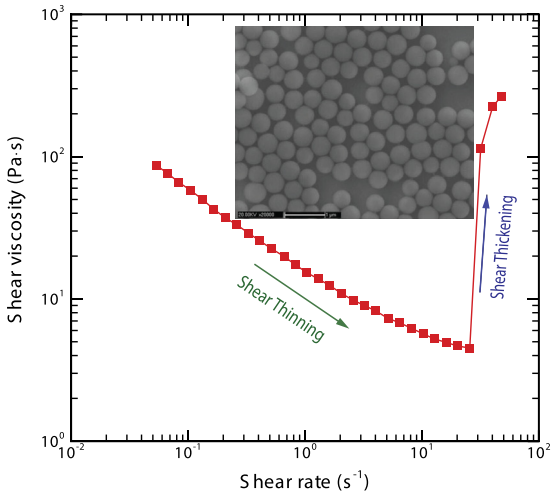


FIG. 2. Steady state shear viscosity of the STF at various strain rates. The decrease and rapid increase of shear viscosities of the STF correspond to the shear thinning and the shear thickening regime, respectively. The inset shows the nearly monodispersed silica sphere particles with an average diameter of 300 nm with less than 10% polydispersity.

the polyethylene glycol are 1.950 g/cm$^3$ and 1.127 g/cm$^3$, respectively. The sound velocity of the silica particles is 5869 m/s. The bulk modulus of the polyethylene glycol is 3.05 GPa, yielding a sound velocity of 1650 m/s. The steady state shear viscosity of the STF at various shear strain rates, which was measured by a Kinexus pro+ rotational rheometer in the steady-state shear sweep mode using a 40 mm 4° cone and plate with Peltier temperature control at 25 °C, was also plotted in Fig. 2. The STF exhibited a shear thinning regime, followed by a strong shear thickening response at a shear rate of about 25 s$^{-1}$ as evident by the sharp increase of the shear viscosity.

### B. Target

The target is assembled by a layer of STF and two aluminum plates, as shown in Fig. 1. The STF is sealed within two 2024 aluminum plates with a size of $\Phi 25.4 \times 0.5$ mm and a 1045 steel gasket with an inner diameter of 21.4 mm with the aid of silicon greases. In the present study, a 0.5-mm-thick steel gasket was used to form a layer of STF specimen with a size of $\Phi 21.4 \times 0.5$ mm. The laser irradiated surface of each assembled target is glued with a 40-$\mu$m-thick aluminum foil as an absorption layer, confined firmly by a 4-mm-thick BK7 glass against the laser irradiation.

### C. Laser

The laser induced shock experiments were performed with a Q-switched high power Nd:YAG pulse laser operating at a wavelength of 1064 nm and a maximum output energy of 2.5 J per shot achieved through a two-step amplification system. The temporal profile of the laser pulse is in the near-Gaussian distribution with a full width at half maximum (FWHM) of about 10 ns. The spatial profile of the laser pulse is modulated to a nearly flat shape. The incident laser beam is focused with a 600 mm optical focal lens to obtain the desired shock diameter.

### D. Measurements

As depicted in Fig. 3, a photonic Doppler velocimetry (PDV) that basically followed the configuration of Strand *et al.*[27] was taken to measure the back free surface velocities of the assembled targets. The PDV consists of a high power 1550 nm CW distributed feedback laser (CQF938 series, provided by JDS Uniphase Corporation) with a polarization maintaining fiber operated at a maximum power of 40 mW with a linewidth of about 200 kHz, a fiber optic circulator, a photodiode detector (InGaAs PIN, provided by New Focus, Inc.) with a bandwidth of 12 GHz, an optical collimating lens probe with back reflection (−13 dB) and a work distance of 15 mm, an oscilloscope (WaveMaster 808Zi, provided by Lecory, Inc.) operating with a bandwidth of 8 GHz and a sampling rate of 40 GSs$^{-1}$ for each channel. The laser and the detector are connected to the first and the third ports of the circulator, respectively, and the probe, which is used to provide the reference light with frequency $f_0$ and collect the Doppler-shifted light with frequency $f_b$ reflected from the moving surface of interest, is connected to the second port of the circulator.

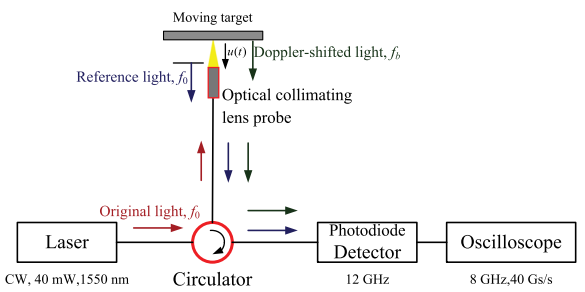


FIG. 3. Configuration of PDV system. The red, the blue, and the green arrows represent the original, the reference, and the Doppler-shifted lights.

The velocity of the measured surface, denoted by $v(t)$, is determined from the difference of the two frequencies, $f_{beat} - f_0$, denoted by $f_{beat}$, as

$$v(t) = \frac{\lambda_0}{2} f_{beat}(t), \tag{1}$$

where $\lambda_0$ is the original wavelength of the CW laser. In the laser induced shock experiments, the measurements are triggered by the temporal domain of the Nd:YAG laser with a Si-biased detector.

### E. Experimental procedure and analysis method

As shown in Fig. 4, while a shock wave with an amplitude of $p_m$ propagates in an assembled target, a part of the wave will reflect due to the impedance mismatch of the aluminum plates and the STF, and some rest of the shock wave will ultimately go through the assembled target and arrive at the back free surface of the right aluminum plate, causing the first peak velocity $v_m$. The consequential peak velocities, which are separated from the first peak, will also arrive at the back free surface due to the multiple reflections of the shock wave in the assembled target. Note that only the elastic waves of the aluminum plates, denoted by a wave speed $C_1$, and a constant wave speed of the STF, denoted by $C_2$, are

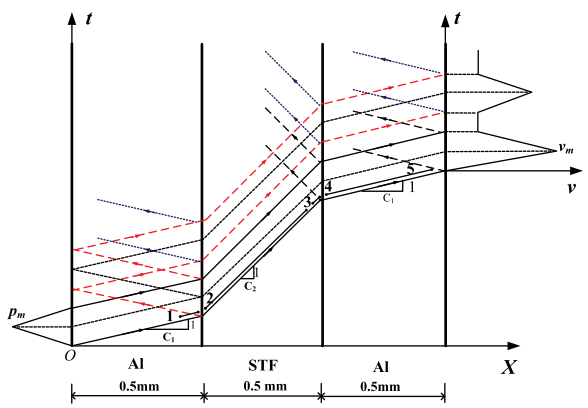


FIG. 4. Characteristic analysis method for analyzing the attenuation behavior of the shock wave in STF based on the measurement results of the back free surface velocities. Note that only the elastic waves of the aluminum plates, denoted by a wave speed $C_1$, and a constant wave speed of the STF, denoted by $C_2$, are depicted to clearly show the analysis method. The velocity profile induced by the shock wave is separated from the consequential velocity profiles induced by the multiple reflections of the shock wave.

given in Fig. 4 to clearly show the analysis method. In the actual analysis, the plastic wave speed is used while the stress exceeds the Hugoniot elastic limit (HEL) of 2024 aluminum material. A characteristic analysis[28] was used to analyze the dynamic response of the STF with the measurement results of the first peak velocity.

The experimental and the analysis procedures are as follows. First, as shown in Fig. 4, the stress at the point 1, denoted by $\sigma_1$, is obtained by measuring the back free surface velocity, $v_{free1}$, of the left aluminum plate directly without the STF specimen and the right aluminum plate. According to the Rankin-Hugoniot relations,[29,30] while $\sigma_1$ is smaller than HEL

$$\sigma_1 = \frac{1}{2}\rho_0 C_e v_{free1}. \tag{2}$$

While $\sigma_1$ exceeds than HEL,

$$\sigma_1 = \rho_0\left(C_0 + S\cdot\frac{1}{2}v_{free1}\right)\cdot\frac{1}{2}v_{free1} + \frac{2}{3}Y_0, \tag{3}$$

where $\rho_0 = 2.77\times10^3\,\mathrm{kg/m^3}$ is initial material density, $C_e = 6.41\times10^3\,\mathrm{m/s}$ is the elastic stress wave velocity, $C_0 = 5.33\times10^3\,\mathrm{m/s}$ is sound velocity at zero pressure, $S = 1.34$ is empirical material parameter, $Y_0 = 265\,\mathrm{MPa}$ is yield stress for 2024Al material,[30–33] respectively, and $\mathrm{HEL} = (1-\nu)Y_0/(1-2\nu) = 547\,\mathrm{MPa}$.

Then, the back free surface velocity of the assembled target, including a thin layer of the STF and the right aluminum plate, denoted by $v_{free2}$, is measured, and the stress at the point 5, $\sigma_5$, is determined while it is smaller than HEL

$$\sigma_5 = \frac{1}{2}\rho_0 C_e v_{free2}. \tag{4}$$

While $\sigma_5$ exceeds than HEL,

$$\sigma_5 = \rho_0\left(C_0 + S\cdot\frac{1}{2}v_{free2}\right)\cdot\frac{1}{2}v_{free2} + \frac{2}{3}Y_0. \tag{5}$$

Since the shock wave will decay in the right aluminum plate, an empirical attenuation law of stress in 2024 aluminum material[21] is undertaken to obtain the stress at the point 4, denoted by $\sigma_4$

$$\frac{\sigma_5}{\sigma_4} = 0.67\exp\left(-\frac{H/2R}{0.71}\right) + 0.25\exp\left(-\frac{H/2R}{0.12}\right) + 0.09. \tag{6}$$

In shock experiments, the thickness of the STF layer was set to be 0.5 mm. The incident energy and the diameter of the Nd:YAG laser were changed to obtain various laser power densities and correspondingly achieve various shock pressures. Note that for a small laser shock diameter, the 2D effect, i.e., the shock wave transformed from uniaxial strain state to dilatation state while propagating in the STF layer, would be obvious.[34,35] Both of bulk compressive effect and shear effect of the STF during laser induced shock were existed in the measured back free surface velocities under this condition. In addition, the impact resistance of the STF layer could be investigated based on the PDV measurements. Here, the nominal impact resistance, $IR_{STF}$, was used to estimate the impact resistance of STF and defined as

$$IR_{STF} = \frac{\sigma_{1\_Peak} - \sigma_{4\_Peak}}{\sigma_{1\_Peak}}\times 100\%, \tag{7}$$

where $\sigma_{1\_Peak}$ and $\sigma_{4\_Peak}$ are incident peak stress at the left aluminum plate, $\sigma_1$, and the transmitted peak stress at the right aluminum plate, $\sigma_4$, respectively.

## III. RESULTS

### A. Velocities of the left aluminum plate at various shock pressures

First, the back free surface velocities, $v_{free1}$, of the left aluminum plate at various shock pressures were measured directly without the STF specimen and the right aluminum plate to obtain the stress, $\sigma_1$, at the point 1, as depicted in Fig. 4. The measured results at various shock pressures and at a same shock diameter of 3.62 mm were given in Fig. 5. It was observed that the peak velocity increased and the shock duration decreased with the increase in the shock pressure. On increasing the shock pressure from 2.59 GPa to 3.82 GPa, the first peak velocity rapidly increased from about 123 m/s to 373 m/s, and the shock duration, defined as the rising duration, $T$, as depicted in Fig. 5, decreased from 53.2 ns to 23.6 ns. Note that the shock pressures for various incident laser power densities were calculated with a previously developed coupling model,[21] in which the fast expansion of laser induced heat plasma and the dynamic deformation of target were analyzed. It was also observed that the plateau duration induced by elastic precursor wave increased with the decrease in the shock pressure, indicating the decrease in the plastic wave speed with the decrease in the shock pressure. In addition, the back free velocities of the first aluminum plate caused by the elastic precursors were about 58 m/s. According to the Rankin-Hugoniot

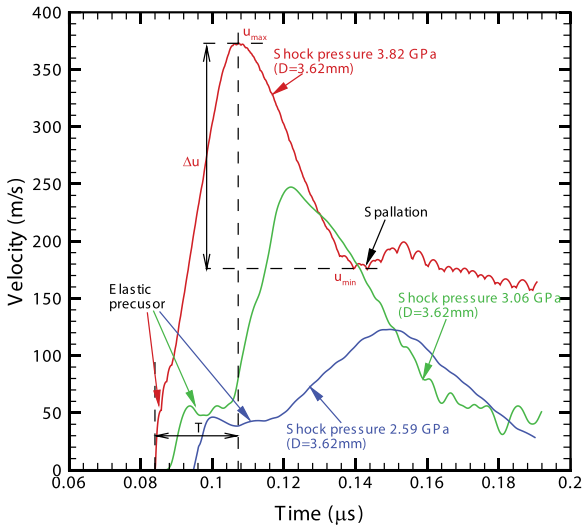


FIG. 5. Measured back free surface velocities of the left aluminum plate at shock pressures of 2.59 GPa, 3.06 GPa, and 3.82 GPa and at the same shock diameter of 3.62 mm. Note that the spallation behavior of 2024 aluminum material was observed for the shock pressure of 3.82 GPa.

relations,[29,30] for the uniaxial strain state, the maximum velocity caused by elastic precursor, $u_{H\_\max}$, could be determined as

$$u_{H\_\max} = \frac{\sigma_{HEL}}{\rho_0 C_e}, \tag{8}$$

where $\sigma_{\mathrm{HEL}}$ is HEL for 2024 aluminum material. From Eq. (8), the maximum velocity caused by the elastic precursor is about 30.8 m/s, which is approximately half of the experimentally measured velocities caused by the elastic precursor wave at the free surface. In addition, the spallation of 2024 aluminum material was observed while shocked at a pressure of 3.82 GPa. The spall strength could be determined as

$$\sigma_{spall} = \frac{1}{2}\rho_0 C_0 \Delta u, \tag{9}$$

where $C_0 = \sqrt{E/3(1-2\nu)\rho_0}$ is the bulk wave speed, and $\Delta u$ is the pull-back velocity defined as the difference between the maximum velocity and the minimum velocity of the spallation signal as depicted in Fig. 5. From Eq. (9), the spall strength of the 2024 aluminum is about 1.40 GPa, which is consistent with the result of Rosenberg *et al.*[36]

### B. Results at a test temperature of 21 °C

The measured back free velocities of the right aluminum plate, $v_{free2}$, with a 0.5-mm-thick layer of the STF at a test temperature of 21 °C and at various shock pressures with a shock diameter of 3.62 mm by means of changing the incident laser energy are given in Fig. 6. Note that the initial slight difference of measured results at a shock pressure of 3.82 GPa should be ascribed to the incompleted interfered fringes induced by elastic precursors. For the PDV measurement, once the measured surface moves a distance of a half of the original wavelength of the CW laser, as depicted in Fig. 3, a complete interfere fringe will be generated. Nevertheless, at some conditions, a complete interfere fringe cannot be obtained while measuring low velocity with short duration such as elastic precursor, leading to the complex of measured data analysis during the determination of the frequency of the incompleted interfered fringes and introducing some errors in the elastic precursor measurement. Except this point, the particle velocity profiles were well measured by the PDV system. For a shock pressure of 3.06 GPa, the small difference in the measured results should be ascribed to the slight difference of STF specimen thicknesses caused by an uncontrolled elastic deformation of the steel gasket while firmly clamping the assembled targets as the previous study.[20] The arriving time increased, i.e., the shock waves speed decreased, with decreasing shock pressure. The previous study[20] showed that the relationship between the shock velocity and the particle velocity in STF at about 21 °C could be described by a similar Grüneisen equation of state (EOS) as $U_s = C_0 + SU_p$[30] with $C_0 = 2.05$ mm/μs and relatively large $S = 5.324$, leading to a higher shock velocity at a higher shock pressure, as shown in Fig. 6. In addition, the first peak velocities decreased rapidly from about 145 m/s to about 8 m/s with decreasing shock pressure from 3.82 GPa to 1.92 GPa.

The measured $v_{free2}$ with a 0.5-mm-thick layer of STF at a test temperature of 21 °C and at various shock pressures by means of keeping almost the same maximum incident laser energies and changing the focused laser diameters are shown in Fig. 7. It could be seen that the first peak velocity slightly increased from about 145 m/s to about 150 m/s with the increase in shock pressure from 3.82 GPa to 4.70 GPa and decreasing shock diameter from 3.62 mm to 2.94 mm. However, the first peak velocity decreased rapidly to about 82 m/s while increasing the shock pressure to 5.38 GPa and decreasing the shock diameter to 2.56 mm. It is to be noted that the shock wave will transform from one dimension state, i.e., uniaxial strain stress wave, to three dimensions state, i.e., dilatational stress wave, while propagating in a relatively thick STF specimen.[35] The bulk viscosity during

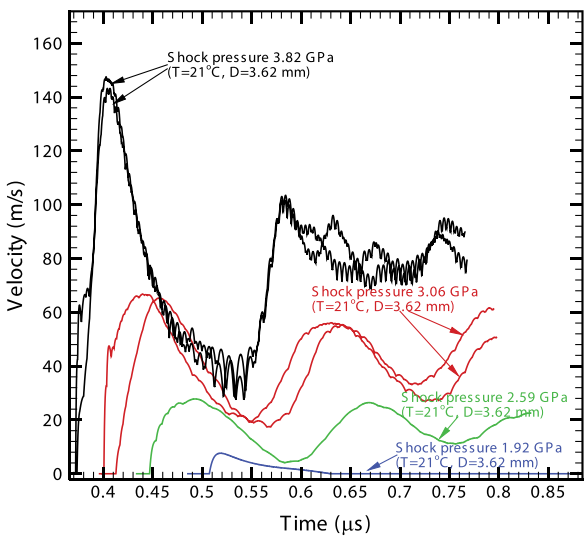


FIG. 6. Measured back free surface velocities of the right aluminum plate with a 0.5-mm-thick layer of STF at a test temperature of 21.0 °C and at various shock pressures with a shock diameter of 3.62 mm.

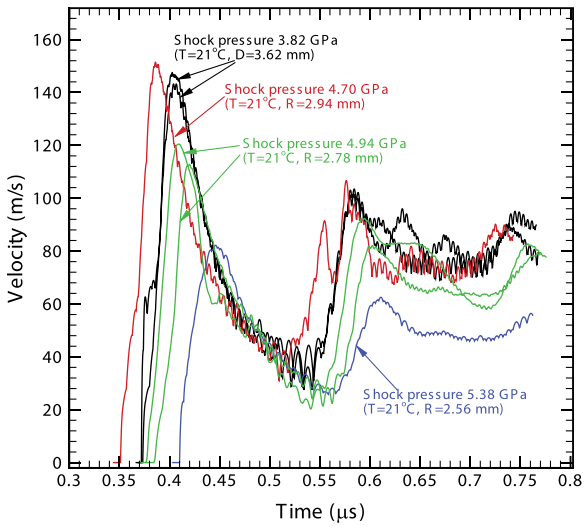


FIG. 7. Measured back free surface velocities of the right aluminum plate with a 0.5-mm-thick layer of STF at a test temperature of 21 °C and at various shock pressures by means of keeping almost the same maximum incident laser energies and changing the focused laser diameters.

compression and the shear viscosity during dilatation should have obvious dragging effects in the STF specimen for the propagations of the aforementioned uniaxial strain stress wave and the dilatational stress wave, respectively. For shock diameters of 3.62 mm and 2.94 mm, the stress wave could be regarded as uniaxial strain stress wave because the shock radii were almost equal to or larger than the thicknesses of assembled aluminum-STF-aluminum targets of about 1.50 mm. Therefore, only the bulk viscosity acted as a dragging mechanism during the propagation of shock waves, leading to the increase of the first peak velocity with increasing shock pressure from 3.82 GPa to 4.70 GPa, as depicted in Fig. 7. However, beside the bulk viscosity, the shear viscosity also acted as a dragging force while the propagation of shock waves with an initial shock diameter of 2.56 mm. Since the first peak velocity decreased significantly for a shock pressure of 5.38 GPa and a shock diameter of 2.56 mm when compared to the results at a shock pressure of 4.70 GPa and a shock diameter of 2.94 mm, it could be speculated that the shear viscosity induced dragging effect was stronger than the bulk viscosity induced dragging effect in the STF at a temperature of 21 °C.

### C. Results at a test temperature of 10 °C

The measured back free velocities of the right aluminum plate, $v_{free2}$, with a 0.5-mm-layer of STF specimen at a temperature of 10 °C and at various shock pressures with a shock diameter of 3.62 mm by means of changing the incident laser energies are shown in Fig. 8. Similarly, the small difference of measured results at the same shock pressure was ascribed to the slight difference of the STF specimens induced by the uncontrolled elastic deformation of the steel gasket while clamping the assembled targets.[20] Similar to the test results at a temperature of 21 °C, the arriving time increased, i.e., the speed of the shock waves decreased, with decreasing shock pressure. In addition, the first peak velocity decreased rapidly from about 108 m/s to about 68 m/s with decreasing shock pressure from 3.76 GPa to 3.04 GPa.

The measured $v_{free2}$ with a 0.5-mm-thick layer of STF at a temperature of 10 °C and at various shock pressures by means of keeping almost the same maximum incident laser energies and changing the focused laser diameters are shown in Fig. 9. Since both the bulk viscosity effect and shear viscosity effect were existed in the STF specimens while shocked at relatively small initial shock diameters, the arriving time was dependent on both the shock pressures and the shock diameters, leading to the unclear tendency of arriving time while increasing the shock pressure and decreasing the shock diameter. In addition, it was observed that the first peak velocity decreased rapidly from about 110 m/s to about 34 m/s with increasing shock pressure from 3.75 GPa to 6.30 GPa and decreasing shock diameter from 3.62 mm to 2.18 mm. As the shear viscosity was obvious for the tests with shock diameters of 2.56 mm and 2.18 mm, the fast decrease of particle velocities for relatively small shock diameters should be ascribed to the shear viscosity induced dragging effect during the propagation of shock waves.

## IV. SUMMARY OF RESULTS AND DISCUSSION

In the present study, the dynamic response of the STF under laser induced shock at various shock pressures, stress states, and test temperatures was investigated by diagnosing the back free surface particle velocities of aluminum-STF-aluminum assembled targets. Fig. 10 shows the summary of the measured back free surface velocities of the right aluminum plate, $v_{free2}$, with a 0.5-mm-thick layer of STF at temperatures of 10 °C and 21 °C and at various shock pressures and diameters. Obvious temperature effect was observed in the experiments except the tests at shock pressures of about 3.05 GPa and at a shock diameter of 3.62 mm. Generally, the relationship between temperature, $T$, and viscosity of viscous fluid, $\eta$, follows the Arrhenius law:

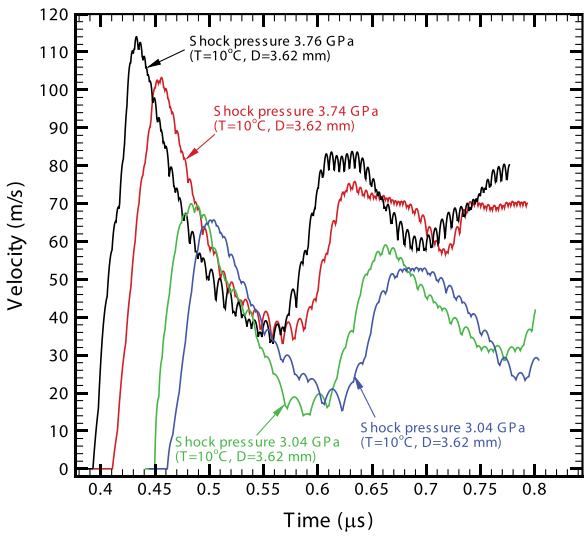


FIG. 8. Measured back free surface velocities of the right aluminum plate with a 0.5-mm-thick layer of STF at a temperature of 10 °C and at various shock pressures with a shock diameter of 3.62 mm by means of changing the incident laser energies.

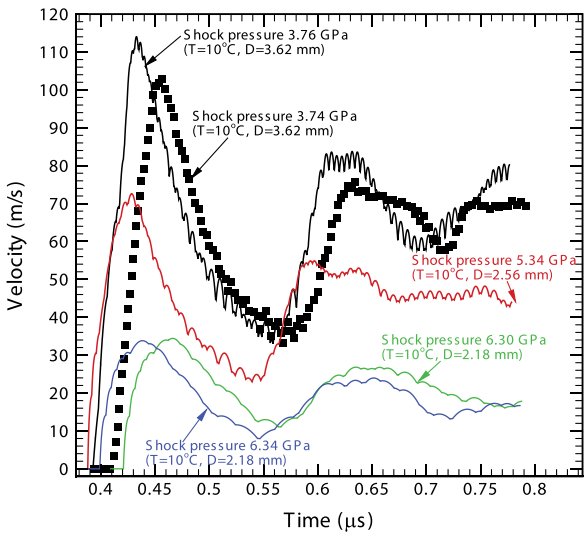


FIG. 9. Measured back free surface velocities of the right aluminum plate with a 0.5-mm-thick layer of STF at a temperature of 10 °C and at various shock pressures by means of keeping almost the same maximum incident laser energies and changing the focused laser diameters.

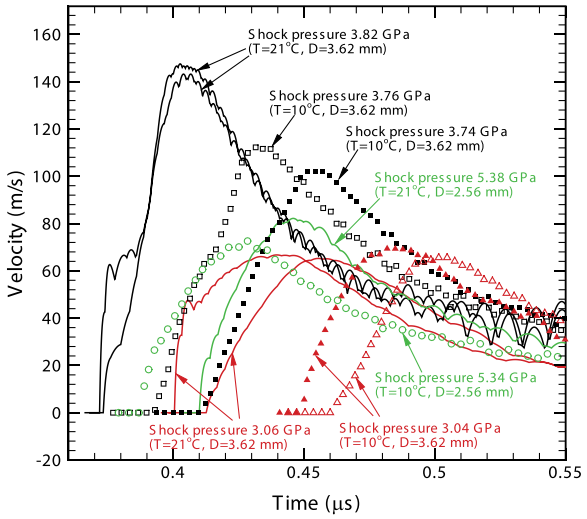


FIG. 10. Summary of measured back free surface velocities of the right aluminum plate with a 0.5-mm-thick layer of STF at temperatures of 21 °C and 10 °C and at various shock pressures and diameters.

$$\eta(T) = \eta_{\text{int}} \exp\left(\frac{E}{RT}\right), \tag{10}$$

where $\eta_{\text{int}}$, $E$, and $R$ are the material viscosity related parameters. Suppose that the temperature-viscosity relationship of the STF also follows the Arrhenius law. From Eq. (10), the viscosity of STF increases with decreasing temperature. As a result, at shock pressures in a range of 3.74 GPa to 3.82 GPa and at a shock diameter of 3.62 mm, the first peak velocity decreases significantly with decreasing temperature from 21 °C to 10 °C. However, the results of 21 °C and 10 °C at the same shock diameter of 3.62 mm are almost identical to each other while decreasing shock pressure to about 3.05 GPa. Since the attenuation behavior of shock waves is mainly ascribed to the bulk viscosity while shocked at a diameter of 3.62 mm, it could be derived that at shock pressures in the range of 3.74 GPa to 3.82 GPa, the bulk viscosity of the STF at the test temperature of 10 °C is much higher than that at the test temperature of 21 °C, and at shock pressures of about 3.05 GPa, it is almost at the same level as the test temperature of 21 °C. The reason should be ascribed to the compression induced thickening behavior of STF during laser induced shock. The study by Waitukaitis and Jaeger[9] showed that the particles inside the suspension were forced across the jamming transient and an impact-jammed solid through the compression of the particle matrix was rapidly growing while a rod impacts the STF directly. The impact induced jamming behavior could also occur during laser induced shock, leading to the rapid stress attenuation by overcoming the short-range hydrodynamic lubrication force between the particles. Once the thickening behavior occurred, the bulk viscosity of STF would be increased significantly. Suppose the impact induced thickening follows a similar shear thickening behavior,

$$\eta_{compression} = \eta_0^{bulk}(T)\dot{\varepsilon}^{\alpha}, \tag{11}$$

where $\eta_0^{bulk}(T)$ is the initial bulk viscosity at temperature $T$, $\dot{\varepsilon}$ is the compressive strain rate, and $\alpha$ is the impact induced thickening exponent. From Eq. (11), the temperature effect on the bulk viscosity of the STF would be amplified by several orders of magnitude after the occurrence of the impact induced thickening behavior. In this regard, it is speculated that the compression induced thickening behavior of the STF occurs at shock pressures higher than 3.74 GPa, and it does not occur at shock pressures lower than 3.06 GPa. The previous studies[9,19,37–40] showed that critical conditions such as a minimum strain were required to obtain the thickening behavior in STF. For the tests with shock pressures about 3.05 GPa and shock diameters 3.62 mm, the minimum strain might be not achieved to occur the impact induced jamming behavior of the STF, leading to the almost identical test results of 21 °C and 10 °C.

It is also observed that the stress state at different shock diameters has a great impact on the dynamic response of the STF, leading to the decrease of peak velocity while increasing the shock pressure and decreasing the shock diameter simultaneously. For a small shock diameter, the shock attenuation behavior of STF depends on both the bulk viscosity and the shear viscosity. Generally, the shear thickening behavior of STF could be described as

$$\eta_{shear} = \eta_0^{shear}(T)\dot{\gamma}^{\beta}, \tag{12}$$

where $\eta_0^{shear}(T)$ is the initial shear viscosity at temperature $T$, $\dot{\gamma}$ is the shear strain rate, and $\beta$ is the shear induced thickening exponent. Therefore, the shear viscosity of STF increases significantly and the temperature effect is amplified by several orders of magnitude once the shear thickening behavior occurs, leading to the sharp decreases of first peak velocities and obvious temperature effect at a relatively small shock diameter of 2.56 mm. The recent study[20] with the same experimental method as the present study, except that a constant shock pressure of about 3.8 GPa and a shock diameter of 3.6 mm were undertaken, showed that the measured free particle velocities of aluminum-STF-aluminum assembled targets were almost identical for the tests at temperatures of 21 °C and 27.2 °C while the thicknesses of STF layer larger than 1.5 mm. As thick layers of STF were taken, the shock waves should also transform from uniaxial strain stress waves to dilatation waves after transmitted to certain distances in the STF specimens. Therefore, the impact induced jamming should be obvious near the shock surface and then the shear induced thickening effect should be obvious after the shock waves transmitted to a certain thickness in STF. However, after the shock waves are transmitted to a relatively long distance, the impact and shear induced thickening behavior should be disappeared because the thickening conditions, such as minimum stress and strain, were not met anymore, leading to the almost saturation behavior of stress and energy absorption and the slight influence of test temperatures in our previous observation.[20]

Fig. 11 shows the relationship between incident peak stress, $\sigma_{1\_Peak}$, and corresponding transmitted peak stress, $\sigma_{2\_Peak}$, at a constant shock diameter of 3.62 mm and at test temperatures of 21 °C and 10 °C. It is observed that the transmitted peak stress increases with increasing incident peak stress for both the test temperatures of 21 °C and 10 °C.

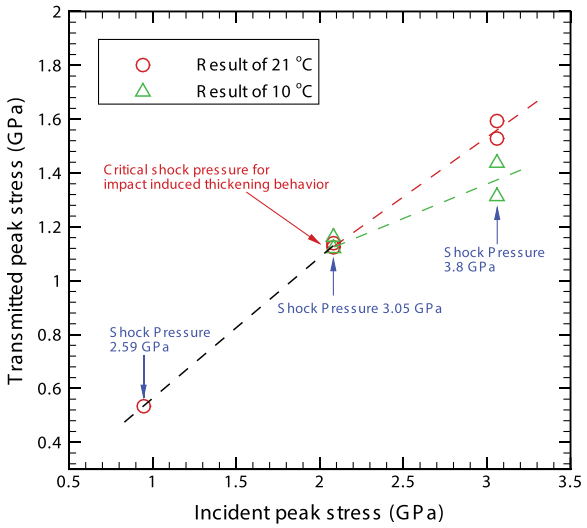


FIG. 11. Relationship between incident peak stress and corresponding transmitted peak stress at a shock diameter of 3.62 mm and at test temperatures of 21 °C and 10 °C. A critical shock pressure for impact induced thickening behavior of STF is observed to be about 3.05 GPa.

However, the increasing velocity of the transmitted peak stress with respect to incident peak stress at a temperature of 10 °C is much slower than that at a temperature of 21 °C. At the highest incident peak stress, i.e., at a shock pressure of about 3.80 GPa, the transmitted peak stress at a temperature of 10 °C is much lower than that at a temperature of 21 °C due to the lower bulk viscosity of STF at the lower temperature after the occurrence of impact induced thickening behavior. Since the compression induce thickening behavior of STF might not occur at a shock pressure of about 3.05 GPa, the transmitted peak stresses are almost at the same level for test temperatures of 21 °C and 10 °C. While the shock pressure is lower than 3.05 GPa, the relationship between incident peak stress and transmitted peak stress should follow the same tendency for the testes at temperatures of 21 °C and 10 °C, which will be validated in future study. According to Eq. (7), at a temperature of 21 °C the nominal impact resistances, $IR_{STF}$, of the layer of STF with a thickness of 0.5 mm are 43.67%, 48.73%, and 50.46% for shock pressures of 2.59 GPa, 3.05 GPa, and 3.80 GPa, respectively, and at a test temperature of 10 °C the nominal impact resistances are 44.24% and 53.02% for shock pressures of 3.05 GPa and 3.80 GPa, respectively. At both test temperatures, the 0.5-mm-thick layer of the STF showed high nominal impact resistance at high pressure. Nevertheless, a relatively narrow temperature range was undertaken to investigate the temperature effects on the dynamic behavior of STF under laser induced shock, further experiments in a wide temperature range will also be conducted in near future. In addition, both the uniaxial and dilatational waves were existed in experiments while shocked at relatively small diameter, making it difficult to isolate the pressure, shear, and temperature effects. The experimental method will be improved in future to investigate the impact induced jamming behavior and shear induced thickening behavior independently.

## V. CONCLUSIONS

In this paper, the dynamic response of the STF under laser induced shock at various shock pressures, stress state, and test temperatures was investigated by measuring the back free surface velocities of aluminum-STF-aluminum assembled targets. The results showed that the attenuation behavior of shock wave in the STF was dependent on the shock pressure, stress state, and test temperature. The measured back free particle velocity of the target and shock wave velocity in the STF is decreased with decreasing shock pressure while shocked at the same temperature and shock diameter. In addition, at a shock diameter of 3.62 mm, the first peak velocity decreased with decreasing test temperature for a high shock pressure of about 3.8 GPa due to the impact induced jamming behavior in the STF, which increased the bulk viscosity and amplified the temperature effect significantly. However, there was not obvious difference between the tests at temperatures of 21 °C and 10 °C and at the same shock diameter of 3.62 mm while decreasing shock pressure to about 3.0 GPa, indicating the bulk induced thickening behavior did not occur in the STF because the shock induced displacements of hard-sphere particles in tens of nanosecond and under such a pressure were not adequate to go across the initial gap of particles. It is also interesting to note that at the same temperature, the particle velocity decreased significantly with increasing shock pressure from about 3.8 GPa to about 5.4 GPa and decreasing shock diameter from 3.62 mm to 2.56 mm, indicating the strong dragging effect induced by the shear induced thickening behavior while the shock wave transformed from uniaxial strain state to dilatation state after transmitted to a certain distance in the STF.

## ACKNOWLEDGMENTS

This paper was supported by National Natural Science Foundation of China under Grant Nos. 11332011 and 11402277. The authors wish to express their appreciation to Professor F. Zhong at Institute of Chemical Materials, China Academy of Engineering Physics for providing the STF material.

[1]P. Lundberg, R. Renström, and B. Lundberg, Int. J. Impact Eng. **24**(3), 259–275 (2000).
[2]C. G. Paalvast, M. L. Verbruggen, and L. B. Vogelesang, EP, EP0237095, A1, 1989.
[3]D. Karagiozova, G. Langdon, and G. Nurick, Int. J. Solids Struct. **49**(19), 2763–2777 (2012).
[4]S. L. Lopatnikov, B. A. Gama, M. Jahirul Haque, C. Krauthauser, J. W. Gillespie, Jr., M. Guden, and I. W. Hall, Compos. Struct. **61**(1), 61–71 (2003).
[5]S. Antonyuk, S. Heinrich, J. Tomas, N. G. Deen, M. S. van Buijtenen, and J. Kuipers, Granul. Matter **12**(1), 15–47 (2010).
[6]C. Daraio, V. Nesterenko, E. Herbold, and S. Jin, Phys. Rev. Lett. **96**(5), 058002 (2006).
[7]R. M. Nedderman, *Statics and Kinematics of Granular Materials* (Cambridge University Press, 2005).
[8]W. Jiang, X. Gong, S. Xuan, W. Jiang, F. Ye, X. Li, and T. Liu, Appl. Phys. Lett. **102**, 101901 (2013).
[9]S. R. Waitukaitis and H. M. Jaeger, Nature **487**(7406), 205–209 (2012).
[10]J. Bender and N. J. Wagner, J. Rheol. **40**(5), 899–916 (1996).
[11]H. Laun, R. Bung, S. Hess, W. Loose, O. Hess, K. Hahn, E. Hädicke, R. Hingmann, F. Schmidt, and P. Lindner, J. Rheol. **36**(4), 743–787 (1992).

[12]M. C. Newstein, H. Wang, N. P. Balsara, A. A. Lefebvre, Y. Shnidman, H. Watanabe, K. Osaki, T. Shikata, H. Niwa, and Y. Morishima, J. Chem. Phys. **111**(10), 4827–4838 (1999).
[13]H. Barnes, J. Rheol. **33**(2), 329–366 (1989).
[14]Y. S. Lee, E. D. Wetzel, and N. J. Wagner, J. Mater. Sci. **38**(13), 2825–2833 (2003).
[15]V. B. C. Tan, T. E. Tay, and W. K. Teo, Int. J. Solids Struct. **42**(5–6), 1561–1576 (2005).
[16]M. J. Decker, C. J. Halbach, C. H. Nam, N. J. Wagner, and E. D. Wetzel, Compos. Sci. Technol. **67**(3–4), 565–578 (2007).
[17]E. V. Lomakin, P. A. Mossakovsky, A. M. Bragov, A. K. Lomunov, A. Y. Konstantinov, M. E. Kolotnikov, F. K. Antonov, and M. S. Vakshtein, Arch. Appl. Mech. **81**(12), 2007–2020 (2011).
[18]R. Helber, F. Doncker, and R. Bung, J. Sound Vib. **138**(1), 47–57 (1990).
[19]A. Lim, S. Lopatnikov, N. Wagner, and J. Gillespie, Jr., Rheol. Acta **49**(8), 879–890 (2010).
[20]X. Wu, F. Zhong, Q. Yin, and C. Huang, Appl. Phys. Lett. **106**(7), 071903 (2015).
[21]X. Wu, Z. Duan, H. Song, Y. Wei, X. Wang, and C. Huang, J. Appl. Phys. **110**(5), 053112 (2011).
[22]X. Wu, Q. Tan, and C. Huang, J. Appl. Phys. **114**(4), 043105 (2013).
[23]X. Wu, C. Huang, X. Wang, and H. Song, Int. J. Impact Eng. **38**(5), 322–329 (2011).
[24]R. Fabbro, J. Fournier, P. Ballard, D. Devaux, and J. Virmont, J. Appl. Phys. **68**, 775–784 (1990).
[25]R. Fabbro, P. Peyre, L. Berthe, and X. Scherpereel, J. Laser Appl. **10**, 265–280 (1998).
[26]X. Hong, S. B. Wang, D. H. Guo, H. X. Wu, J. Wang, Y. S. Dai, X. P. Xia, and Y. N. Xie, Opt. Lasers Eng. **29**(6), 447–455 (1998).
[27]O. Strand, D. Goosman, C. Martinez, T. Whitworth, and W. Kuhlow, Rev. Sci. Instrum. **77**, 083108 (2006).
[28]L. Wang, *Foundations of Stress Waves* (Elsevier, 2011).
[29]P. C. Chou and A. K. Hopkins, *Dynamic Response of Materials to Intense Impulsive Loading* (Air Force Materials Laboratory, Wright Patterson AFB, OH, 1972).
[30]M. A. Meyers, *Dynamic Behavior of Materials* (Wiley-Interscience, 1994).
[31]G. R. Johnson and W. H. Cook, Presented at the Proceedings of 7th International Symposium on Ballistics, 1983.
[32]M. Meyers, *Dynamic Behavior of Materials*, 1st ed. (Wiley-Interscience, New York, 1994).
[33]G. Johnson and W. Cook, Presented at the Proceedings of the 7th International Symposium on Ballistics, The Hague, The Netherlands, 1983.
[34]J. A. Bolger, C. S. Montross, and A. V. Rode, J. Appl. Phys. **86**(10), 5461–5466 (1999).
[35]M. Boustie, J. P. Cuq-Lelandais, C. Bolis, L. Berthe, S. Barradas, M. Arrigoni, T. D. Resseguier, and M. Jeandin, J. Phys. D: Appl. Phys. **40**(22), 7103 (2007).
[36]Z. Rosenberg, G. Luttwak, Y. Yeshurun, and Y. Partom, J. Appl. Phys. **54**(5), 2147–2152 (1983).
[37]J. W. Bender and N. J. Wagner, J. Colloid Interface Sci. **172**(1), 171–184 (1995).
[38]R. Hoffman, J. Colloid Interface Sci. **46**(3), 491–506 (1974).
[39]B. J. Maranzano and N. J. Wagner, J. Rheol. **45**(5), 1205–1222 (2001).
[40]B. J. Maranzano and N. J. Wagner, J. Chem. Phys. **114**(23), 10514–10527 (2001).